



In vitro galactose-targeted study of RSP050-loaded micelles against liver hepatocellular carcinoma

Anisha Mazumder, Anupma Dwivedi, Wirat Assawapanumat, Runghapha Saeeng, Witaya Sungkarat & Norased Nasongkla

To cite this article: Anisha Mazumder, Anupma Dwivedi, Wirat Assawapanumat, Runghapha Saeeng, Witaya Sungkarat & Norased Nasongkla (2022) *In vitro* galactose-targeted study of RSP050-loaded micelles against liver hepatocellular carcinoma, Pharmaceutical Development and Technology, 27:4, 379-388, DOI: [10.1080/10837450.2022.2063891](https://doi.org/10.1080/10837450.2022.2063891)

To link to this article: <https://doi.org/10.1080/10837450.2022.2063891>



Published online: 18 May 2022.



Submit your article to this journal [↗](#)



Article views: 40



View related articles [↗](#)





View Crossmark data [↗](#)

RESEARCH ARTICLE



In vitro galactose-targeted study of RSPP050-loaded micelles against liver hepatocellular carcinoma

Anisha Mazumder^a, Anupma Dwivedi^a, Wirat Assawapanumat^a, Rungnapha Saeeng^b, Witaya Sungkarat^c  and Norased Nasongkla^{a,d} 

^aDepartment of Biomedical Engineering, Faculty of Engineering, Mahidol University, Nakorn Pathom, Thailand; ^bDepartment of Chemistry, Faculty of Science, Burapha University, Saen Suk, Thailand; ^cDepartment of Radiology, Faculty of Medicine, Ramathibodi Hospital, Mahidol University, Bangkok, Thailand; ^dDepartment of Chemistry and Center of Excellence for Innovation in Chemistry, Faculty of Science, Mahidol University, Bangkok, Thailand

ABSTRACT

Andrographolide is a group of diterpenoid lactone isolated from *Andrographis paniculata* (Burm. F.) NEES. One of the analogues is 19-O-triphenylmethylandrographolide (RSPP050) which possesses anticancer activity. In seeking to capitalise on the last property, we have investigated the *in vitro* tumour targeting capabilities and MRI imaging for hepatocellular carcinoma. In this study, we have designed galactose-targeted and non-targeted micelles comprised of poly(ethylene glycol)-b-poly(lactide) that enveloped RSPP050 as an anticancer agent and superparamagnetic iron oxide (SPIO) as a contrast agent. The targeting abilities were endeavored by examining the cellular uptake with MTT assay, fluorescence microscopy, Prussian blue staining, and *in vitro* MRI. Targeted SPIO micelles as a T2* contrast agent decreased the relative T2* MRI intensity at 3 h. Results revealed that galactose micelles displayed $10.91 \pm 0.19\%$ drug loading content, -37.17 ± 0.63 mV zeta potential, and these micelles at the concentration of 0.5 $\mu\text{g/ml}$ exhibited higher cytotoxicity than non-targeted micelles and free RSPP050 after incubation for 24 h. Fluorescence microscopy and Prussian blue staining at 3 h demonstrated significant cellular uptake by HepG2 cells. Thus, anticancer activity of RSPP050 could be improved using galactose as a targeting ligand and theranostic function was achieved using SPIO.

ARTICLE HISTORY

Received 11 September 2021
Accepted 4 April 2022

KEYWORDS

RSPP050; galactose targeted micelles; SPIO micelles; *in vitro* anticancer; *in vitro* MRI; HepG2

1. Introduction

Andrographis paniculata (Burm. F) Nees, a herbaceous plant is native to South East Asia and possessed by the Acanthaceae family. Andrographolide (diterpenoid lactone) is one of its major bio-active compounds and bear numerous biological properties such as immunostimulatory, anti-inflammatory, anti-allergic, anti-bacterial, anti-tumour, anti-viral, anti-malarial, hepatoprotective, and antidiabetic (Kumar et al. 2004; Jayakumar et al. 2013). Andrographolide exerts low therapeutic efficiency for inhibiting cancer cells and can be ameliorated by altering its chemical structure (Eawsakul et al. 2017). One such known modified andrographolide is RSPP050 among many and known to exert its cytotoxic effects against cancer cells (Sirion et al. 2012; Bhummaphan et al. 2013; Eawsakul et al. 2017).

During recent decades, theranostic agents have allured stupendous interest which has been deployed to ameliorate therapeutic efficacy by facilitating the therapeutic agents to the tumour site and also for amalgamation of cancer detection and therapy. Antecedently many researchers have inspected that theranostic nanocarriers can be attached with functional agents and ligands for targeting various cancer cells, employing anticancer drugs and diagnostic agents for the detection and monitoring of the targeted therapy (Nasongkla et al. 2004; Schleich et al. 2013; Yang et al. 2017). The third most fatal cancer with a survival period of about six months is known to be hepatocellular carcinoma (HCC)

(El-Serag and Rudolph 2007; Pranatharthihran et al. 2017). It predominantly affects hepatocytes which are known to be more than 80% of the hepatic cells (Poelstra et al. 2012). Rapid detachment of particulate carriers by kupffer cells restricts the hepatocyte aggregation, thus hampering therapeutic ability. Henceforth, targeted delivery elucidates a vital approach for liver cancer treatment and can be accomplished by targeted delivery to receptors which are profusely present on hepatocytes (Iacobazzi et al. 2017). The Ashwell-Morell Receptor (ASGPR), is a liver related surface receptor and circa 500 000 receptor per cell are majorly residing on hepatocytes and are abundantly expressed on well differentiated form of HCC (Fallon and Schwartz 1988; Hyodo et al. 1993). It is documented that ASGPR is associated in the clearance of glycoproteins with galactose or acetylgalactosamine residues from circulation with the aid of clathrin type receptor mediated endocytosis (Iacobazzi et al. 2017). After formation, the ligand-ASGPR receptor is promptly internalised and the receptor comes back to the surface facilitating superior binding affinity and puissant cellular uptake of ligand (Ciechanover et al. 1983). Results of cellular uptake by Feng et al. (2014) indicated that the galactose targeted micelles effectively transferred doxorubicin to HepG2 cells via ASGPR mediated endocytosis. Huang et al. (2017) research also suggested that galactose nanoparticles recognise ASGPR on hepatocellular carcinoma cell (HepG2) surface, and expedite its uptake by virtue of inner-mediated endocytosis. It is established that clathrin and caveolae-mediated endocytosis and

macropinocytosis are responsible for internalisation of micelles into the cells.

Polymeric micelles as nanocarriers can be attached with targeting ligands to deliver payloads and increases its potential at the tumour site specific targets and also enhance their tumour-selectivity via augmented permeability and retention (EPR) effect. In the micellar core-shell structure, the inner hydrophobic core can be encapsulated with hydrophobic agents, whilst their hydrophilic shell enables stabilisation in a hydrophilic milieu, allowing them to self-assemble in an amphiphilic block copolymers (Yoo et al. 2002; Situ et al. 2016). Poly(ethylene glycol) (PEG) is the most broadly used outer shell, as it carries advantages like antiphagocytosis against macrophages, immunogenicity, biocompatibility hydrophilicity, non-toxic, protection of protein absorption and immune recognition, more blood circulation time (Xiao et al. 2010; Ebrahimi et al. 2016). The hydrophobic polymers generally used are poly(lactide) (PLA), they function as inner core and aids in accommodating hydrophobic drugs and provides stability and assist in improving solubility (Theerasilp and Nasongkla 2013). Superparamagnetic iron oxide (SPIO) nanoparticles are propitious nanoplateforms for contrast-enhanced MRI and the latter offers an excellent contrast agent for soft tissue at better resolution and is mostly modality to identify malignant and normal tissue (Brigger et al. 2002). They have renowned characteristics of exhibiting non-toxicity, biocompatibility and an outstanding magnetic trait (used as MRI probes) (Situ et al. 2016). Due to deficiency in uptake of SPIO by specific cells, stability issues, poor efficiency of internalisation and low sensitivity polymeric micelles as multifunctional platform for delivering drugs, diagnosis, imaging, and SPIO nanocarrier system has been utilised (Fan et al. 2011). In the mouse model, SPIO polymeric micelles displayed no systemic toxicity and proved its multifunctionality for cancer therapy and detection using MRI (Thitichai et al. 2019). Nasongkla et al. designed polymeric micelles as cancer targeting abilities with $\alpha v \beta 3$ integrins and SPIO as contrast agent (Nasongkla et al. 2006). SPIO lowers the proton relaxation time and is a powerful proton relaxation enhancer. It has an effect on high spin-spin (T_2) relaxivity (Ai et al. 2005; Cheng et al. 2011).

Previously, our research group have investigated the *in vitro* anticancer effects of RSPP050 and also encapsulated into the polymeric micelles to increase its aqueous solubility, bioavailability and enhanced cytotoxic activity against cholangiocarcinoma (Puntawee et al. 2016; Eawsakul et al. 2017). Hence, it was of our interest in evaluating the HCC-targeting activities of the galactose-SPIO-RSPP050 micelles by *in vitro* studies, and to further investigate the feasibility for *in vitro* MRI. Our research proposed to construct micelles with galactose moiety as a theranostic agent, wherein RSPP050 act as an anticancer drug and SPIO nanoparticles as an imaging contrast agent. RSPP050/SPIO micelles decorated with galactose were fabricated to target HepG2 cancer cells through asialoglycoprotein receptor (ASGPR) in the *in vitro* target system. Furthermore, the cellular uptake of these galactose targeted SPIO and non-targeted SPIO micelles was investigated and also endeavoured for MRI. We also assessed these SPIO micelles on L929 mouse fibroblast (normal cells). To our best knowledge, *in vitro* ligand targeted efficacy, anticancer effects and MRI of novel analogue; RSPP050 has not been explored.

2. Materials and methods

2.1. Materials

Galactose-PEG(4K)-b-PLA(3K) and allyl-PEG(4K)-b-PLA(3K) polymers were purchased from NanoPolyPEG, Co. Ltd. (Bangkok, Thailand).

Prof. Rungnapha Saeeng (Department of Chemistry, Faculty of Science, Burapha University, Saen Suk, Thailand) provided RSPP050 (anticancer drug used in this research work). Nile red was purchased from TCI (Tokyo, Japan) and potassium ferrocyanide and glutaraldehyde solution from Sigma-Aldrich (St. Louis, MO). All the solvents used for the experimental purpose were procured from RCI Labscan (Bangkok, Thailand).

2.2. Determination of the RSPP050/SPIO/Nile red loading contents

SPIO micelles were freeze-dried and then disseminate in ethanol prior to UV-vis analysis. In order to segregate the suspending SPIO nanoparticles, a bar magnet was kept on the samples overnight. NanoDrop™ UV-Vis spectrophotometer (Thermo Fisher Scientific, Waltham, MA) was used to analyse RSPP050. RSPP050 with different concentrations was dissolved in ethanol and the absorbance was noted at 252 nm.

Flame atomic absorption spectrophotometer (FAAS) (Perkin Elmer, Waltham, MA) was deployed to determine the iron (Fe) content of SPIO micelles. For the micelle disaggregation and disintegration of SPIO nanoparticles, the samples were dripped into HCl solution for about 20 min. At the absorption wavelength of 248.3 nm, iron concentration was spotted. The formulae for calculating drug loading content (%) and drug loading efficiency (%) are given below:

$$\begin{aligned} \text{Drug loading content (\%)} &= \frac{\text{weight of drug in micelles (mg)}}{\text{weight of micelles (mg)}} \times 100 \\ \text{Drug loading efficiency (\%)} &= \frac{\text{amount of drug in micelles (mg)}}{\text{initial amount of drug (mg)}} \times 100 \end{aligned}$$

For Nile red samples, SPIO micelles were well dissolved in ethanol and for separating SPIO nanoparticles the samples were attached with a magnetic bar overnight. Fluorescence spectroscopy at excitation 559 nm and emission 617 nm was used to measure the Nile red content.

2.3. Preparation of galactose RSPP050/SPIO micelles (targeted) and allyl RSPP050/SPIO micelles (non-targeted) and Nile red loaded micelles

Galactose-PEG-b-PLA, SPIO and RSPP040 were completely dissolved in tetrahydrofuran (THF) via vortex and then the above concoction was drop wise added to the deionised water in the presence of ultrasonic probe sonication (SONIC, Model VCX 130, Newtown, CT) to acquire micelles in the aqueous milieu. These micelles were placed on top of orbit shaker and to remove the traces of solvent in the micelle solutions air pump was utilised. In order to remove free drug, micelles were filtered by 0.45 μm filters and was centrifuged (centrifugal filter M_w cut off 50 kDa) at 4000 rpm at 4 °C. For preparing non-targeted micelles, allyl-PEG-b-PLA polymer was utilised.

For preparing Nile red micelles, galactose-PEG-b-PLA, SPIO, RSPP040, and Nile red were dissolved together in THF and the above blend was dropped into the DI water deploying ultrasonic probe. For preparing allyl Nile red micelles, allyl-PEG-b-PLA was used.

2.4. Transmission electron microscopy (TEM)

TEM samples were prepared by adding a drop of SPIO micelles samples on to carbon coated copper grids and excess were removed by filter paper and dehydrated completely. SPIO micelles were spotted and captured under JEM-2010 electron microscope at an accelerating voltage of 200 kV, LaB6 filament and a bottom mounted Gatan CCD camera.

2.5. Measurement of particle size and zeta potential

For measuring the size and zeta potential of RSPP050/SPIO micelles and SPIO micelles, dynamic laser light scattering (DLS) at 25°C with Zetasizer Nano ZS, Malvern (Worcestershire, UK) was utilised.

2.6. Preparation of SPIO nanoparticles

SPIO nanoparticles preparation method was followed as previously reported (Mazumder et al. 2019). In the presence of nitrogen gas, oleic acid (6 mmol), oleylamine (6 mmol), Fe(acac)₃ (2 mmol), benzyl ether (20 ml), and 1,2-hexadecanediol (10 mmol) were blended together in a round bottom equipped with condenser for refluxing and heated up to 200°C for 2 h. Temperature was then increased to 300°C for 1 h. The product was precipitated in ethanol and separated by centrifugation. Hexane was added to resuspend this precipitate.

2.7. Culturing of human hepatocellular carcinoma (HepG2) and mouse fibroblast (L929) cell line

HepG2 and L929 cell line obtained from JCRB cell bank (Osaka, Japan) were cultured at 37°C in a 5% CO₂ humidified environment and using Dulbecco's modified Eagle's medium (DMEM) as a cell culture media for HepG2 and minimum essential medium (MEM) for L929. Cell culture media was added by 10% foetal bovine serum (Biochrom, Berlin, Germany) and 1% penicillin/streptomycin (Gibco, Carlsbad, CA). Both cells were cleaned twice with sterile phosphate-buffered saline (PBS) followed by trypsin-EDTA solution (Biochrom, Berlin, Germany) for 5 min at 37°C to detach all the cells. Then, cell pellets were obtained by centrifugation at 1500 rpm, 4°C for 6 min. Fresh culture media was added to the pellet and mixed well after the disposal of supernatant. In every alternative day, the culture medium was replenished with fresh media. Cell viability was monitored and calculated by employing trypan blue test and viability was calculated by the formulae below:

Viable cells (%)

$$= \text{number of live cells} / \text{total cells (live + dead cells)} \times 100$$

2.8. In vitro cytotoxic assay

In vitro cell viability of SPIO micelles against HepG2 and L929 cells was evaluated by deploying MTT assay. MTT solution at the concentration of 2 mg/ml was prepared using serum free medium. For monolayer formation, HepG2 and L929 (20 000 cells/well) were pipetted into 96-well plates, incubated for 24 h and treated with different concentrations of RSPP050 (in 5% DMSO), galactose SPIO micelles (targeted), allyl SPIO micelles (non-targeted) blank SPIO micelles (without RSPP050), and DMSO (5%). After 24 h, the medium was discarded and the MTT solution (50 µl) was added. The plate was placed in 5% CO₂ humidified incubator at 37°C for

around 1.5 h. After 1.5 h, MTT solution was taken out and discarded, followed by addition of 200 µl of DMSO and mixed well. The absorbance was noted and recorded at 570 nm using a VERSA max microplate reader (Molecular Devices, CA, USA). The percentage cell viability was calculated by using the formulae below:

% Cell viability

$$= \text{absorbance of treated cells} / \text{absorbance of the untreated cells} \times 100$$

2.9. Cellular uptake of Nile red loaded SPIO micelles

For imaging the cellular uptake, HepG2 and L929 cells at the density of 50 000 cells/well were seeded in glass bottom dishes for 24 h. The media was then aspirated and cells were washed by sterilised PBS without disturbing cells followed by addition of serum-free medium to the well plates. Galactose and allyl RSPP050/SPIO/Nile red loaded micelles were added to the wells at Nile red concentration of 0.02 µg/ml and incubated at 37°C for 0.5, 1, and 3 h. After incubation at various time periods, the medium was removed and cells were washed with PBS to withdraw the excess micelles. For fixing the cells, 2.5% glutaraldehyde was used for 20 min, after 20 min cells were subjected to wash with PBS, following incubation with Hoechst (12 µl/ml) solution for 20 min. Then, the solution was discarded and rinsed with PBS several times. The images were captured and examined under fluorescence microscopy (Eclipse Ti-S Nikon, Tokyo, Japan). Images J was employed to measure the fluorescence intensity.

2.10. Prussian blue staining and intracellular iron content

For Prussian blue staining, HepG2 and L929 cells (50 000 cells/well) were seeded into the well plate for 24 h then cells were washed with PBS and serum free media. Galactose targeted and non-targeted SPIO micelles were incubated for 0.5, 1, and 3 h at 37°C in 5% CO₂ humidified atmosphere at the iron concentration of 61 ppm. After incubation at various time period, cells were rinsed by PBS in order to remove free iron particles. To fix the cells, 2.5% glutaraldehyde solution was incubated for 20 min following incubation, the cells were washed with PBS. Then, the cells were incubated at 37°C with 10% potassium ferrocyanide and 20% HCl solution for 45 min. After that, cells were washed by PBS three times then images of Prussian blue staining were captured under bright field inverted microscopy (Eclipse Ti-S Nikon, Tokyo, Japan).

For intracellular iron content study, 50 000 cells/well of HepG2 cells were seeded into 24-well plate. After incubation for 24 h, the media was removed. Cells were washed with PBS and fresh serum free media was seeded into the well plate. Galactose targeted and non-targeted SPIO micelles were incubated at 0.5, 1, and 3 h time period with an iron concentration of 61 ppm. After incubation, media was removed and cells were trypsinised and proceeded by centrifugation for 1500 rpm for 10 min at 4°C. Solutions of 12 M HCl were added to the cells which were collected after centrifuge, iron content in these solutions was measured by using flame atomic absorption spectroscopy.

2.11. In vitro MRI

In six-well plate, HepG2 cells with 5×10^5 per well were seeded and incubated for 24 h. After 24 h of monolayer formation, cells were incubated with galactose targeted and allyl non-targeted

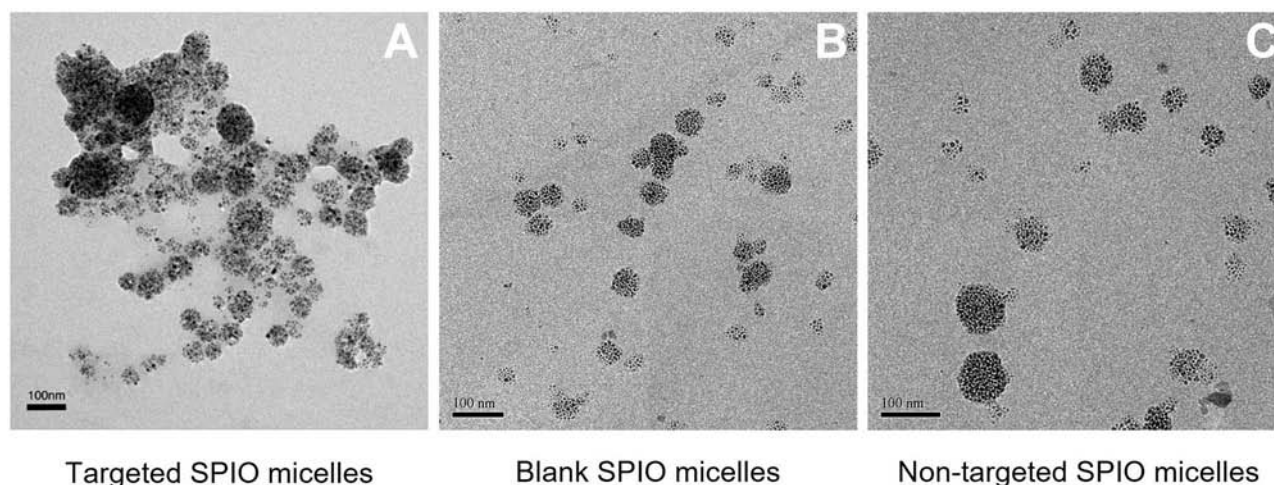


Figure 1. TEM micrographs depict (A) targeted SPIO micelles, (B) blank SPIO micelles, and (C) non-targeted SPIO micelles at $\times 25\,000$ magnification. The scale bar represents 100 nm.

SPIO micelles for 3 h in a humidified atmosphere with 5% CO_2 at 37°C . After that cells were cleaned with PBS, trypsinised and centrifuged at 1500 rpm for 8 min at 4°C . For fixing cells, 2.5% glutaraldehyde solution was utilised for about 30 min. Following fixation, cells were centrifuged and then PBS was added to the cells and suspended well and to this PBS, 2% agarose solution was added and transferred to 96 well plates, which was employed as MRI phantom. Phantom well plates were placed at 4°C overnight. Phantom was scanned by a 3-Tesla MRI scanner with high magnetic field strength (Ingenia, Philips, The Netherlands, B.V., Best, The Netherlands) equipped with an elbow coil (dStream, Philips, Netherlands, B.V., Best, The Netherlands).

2.12. Statistical analysis

GraphPad Prism™ (version 5.01, La Jolla, CA) was deployed for statistical analysis and the experiments were performed in triplicate. Statistical significance was interpreted with one-way ANOVA. Results are illustrated as mean \pm standard deviation (SD), and significance was at $p < 0.05$.

3. Results and discussion

3.1. Characterisation of galactose RSPP050/SPIO micelles and allyl RSPP050/SPIO micelles

Galactose and allyl RSPP050/SPIO-loaded micelles were prepared by solvent evaporation method as published earlier (Theerasilp et al. 2018; Mazumder et al. 2019). SPIO micelles were assessed for their zeta potential, particle size, encapsulation efficiency, drug loading content, polydispersity index (PDI), and iron content. DLS measurement shows that the size of targeted and non-targeted SPIO micelles was 141.5 ± 15.56 and 160.6 ± 10.47 nm, respectively. Size of blank micelles was 131 ± 7.93 nm and was smaller than targeted and non-targeted SPIO micelles, as no drug (RSPP050) was loaded into the hydrophobic core of blank micelles. It has also been reported that nanoparticles with less than 200 nm in size have extravasation and accumulation at tumour site by the enhanced permeability and retention (EPR) effect (Li M et al. 2016). Yang et al. (2017) prepared SPIO micelles with amphiphilic diblock polymer with galactosyl and lactosyl sugar units as a target ligand (ASGPR) and found that the size of micelles was 120 and 150 nm, respectively. In another study, polymeric micelles were conjugated with folate and were examined for tumour

targeting by MRI. Particle size of these micelles was reported at 196 nm (Li H et al. 2015). In the present study, zeta potential was found to be -37.17 ± 0.63 mV for targeted SPIO micelles. The size of non-targeted and blank SPIO micelles was at -34.57 ± 0.70 and -36.33 ± 1.26 mV, respectively. It was reported that micelles with negative zeta potential caused electrostatic repulsion in the particles, provided stability and prevented aggregation during physiological conditions. Negatively charged particles prolong blood circulation time and lower the chance of non-specific binding to normal cells (Voon et al. 2017). Galactose SPIO micelles displayed drug loading content and drug loading efficiency at $10.91 \pm 0.19\%$ and $19.28 \pm 0.35\%$ whilst non-targeted SPIO micelles displayed drug loading content and drug loading efficiency at $11.33 \pm 0.47\%$ and $17.65 \pm 0.74\%$. Next, iron content in micelles was evaluated. Results show that iron content of galactose targeted, non-targeted SPIO and blank SPIO micelles was 1.51 ± 0.03 , 1.54 ± 0.04 , and 1.64 ± 0.07 mg, respectively. Polydispersity index of these micelles is small: targeted SPIO micelles 0.18 ± 0.03 , blank SPIO micelles 0.18 ± 0.04 , and non-targeted SPIO micelles 0.14 ± 0.01 . In the current study, the particle size of SPIO nanoparticles was approximately 5 nm in diameter. It should be noted that an ideal iron oxide nanoparticles to be categorised as superparamagnetic should have diameter in the range of 4–10 nm (Lam et al. 2013).

3.2. Transmission electron microscopy

TEM was exploited to examine the size and morphology of RSPP050/SPIO-loaded micelles (Figure 1). TEM micrographs of targeted, blank, and non-targeted SPIO micelles are shown in Figure 1(A–C). It was visualised that targeted, non-targeted, and blank SPIO micelles exerted spherical shape with no indication of aggregation. SPIO nanoparticles can be indicated as the black spot encircled by dark grey area. Results also showed that SPIO nanoparticles were encapsulated into the hydrophobic core of polymeric micelles. For blank SPIO micelles (without drug), no drug was encapsulated into the hydrophobic core, consequently the size was smaller.

3.3. In vitro cytotoxicity

HepG2 and L929 cell lines were exploited to demonstrate the cytotoxic effects of the blank SPIO, targeted SPIO and non-

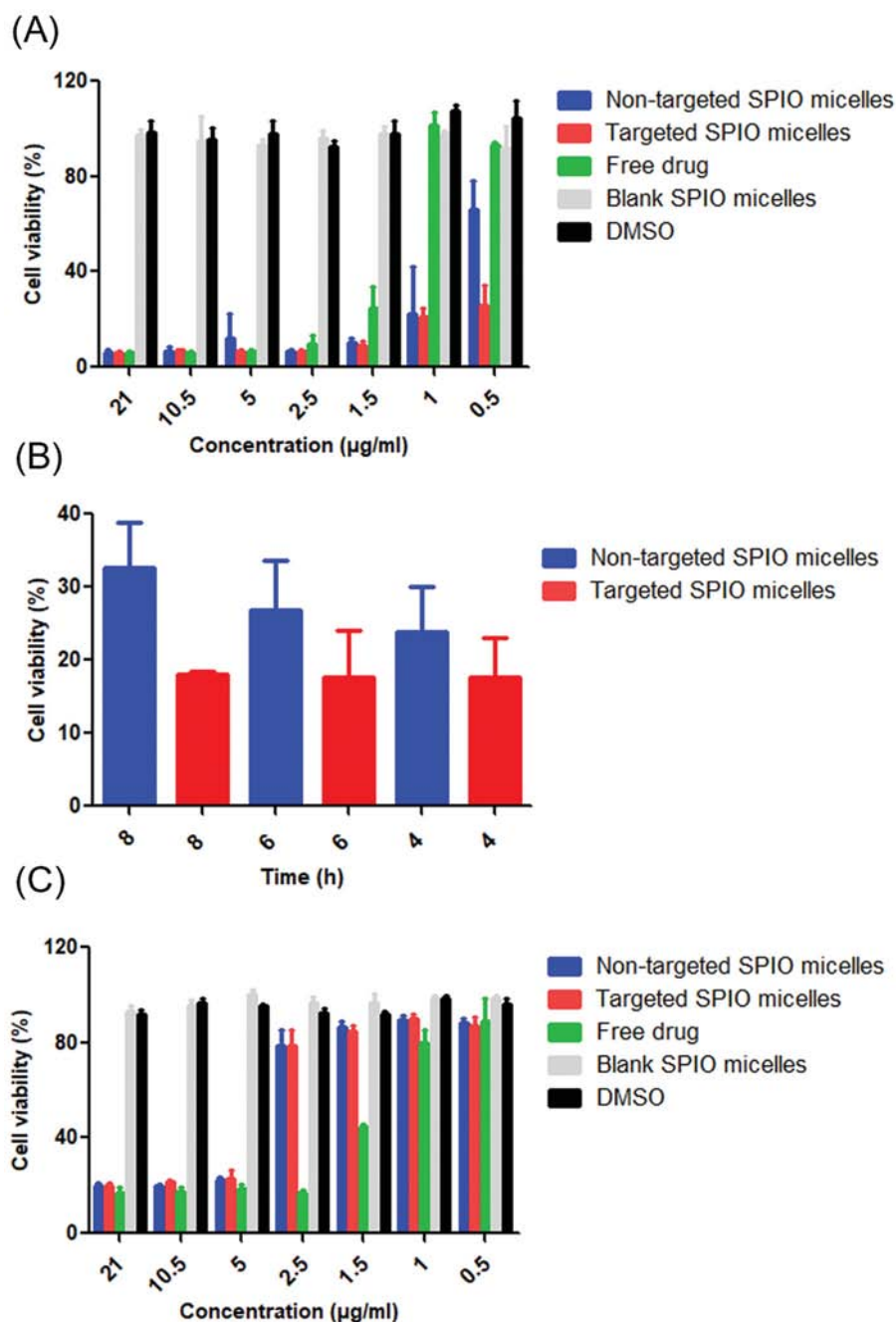


Figure 2. *In vitro* cell viability of HepG2 and L929 cells. (A) Cell viability against HepG2 after 24 h of incubation of targeted, blank and non-targeted SPIO micelles, free drug, and DMSO with different concentrations (21, 10.5, 5, 2.5, 1.5, 1, and 0.5 µg/ml). (B) Cytotoxicity of targeted and non-targeted SPIO micelles against HepG2 incubated at various time periods at concentration 21 µg/ml. (C) Cell viability against L929 after 24 h of incubation of targeted, blank and non-targeted SPIO micelles, free drug, and DMSO with various concentrations (21, 10.5, 5, 2.5, 1.5, 1, and 0.5 µg/ml). Data represent the mean \pm standard deviation ($n = 3$).

targeted SPIO micelles, free drug and DMSO (Figure 2). HepG2 and L929 cells were treated with various concentrations of SPIO micelles (21, 10.5, 5, 2.5, 1.5, 1, and 0.5 µg/ml), free RSPP050 and DMSO. After 24 h, MTT assay was carried out to assess the cell viability. The viability of HepG2 cells (Figure 2(A)) was almost 100% for all concentrations of blank SPIO micelles as confirmed by the *in vitro* cell proliferation assay. These results confirmed that biodegradable PEG-PLA SPIO-micelles are non-toxic and did not induce any inhibitory effects. It was noteworthy that galactose targeted micelles exerted cytotoxic effects at almost all concentrations (Figure 2(A)). Non-targeted SPIO micelles at all

concentrations except the lowest concentration (0.5 µg/ml) inhibited the growth of HepG2 cells. Free RSPP050 did not elicit toxic effects at lower concentration (0.5 and 1 µg/ml) but it showed cytotoxic effects at other concentrations (21, 10.5, 5, 2.5, and 1.5 µg/ml). At the concentration of 0.5 µg/ml, it was noticed that galactose targeted SPIO micelles exhibited significant (one-way ANOVA, $p < 0.05$) toxic effects than non-targeted micelles after 24 h of incubation time. In order to test the cytotoxic effects and later cellular uptake study of targeted and non-targeted micelles with lesser incubation period than 24 h, we decided to assess cytotoxic activity at higher concentration (21 µg/ml) with lesser

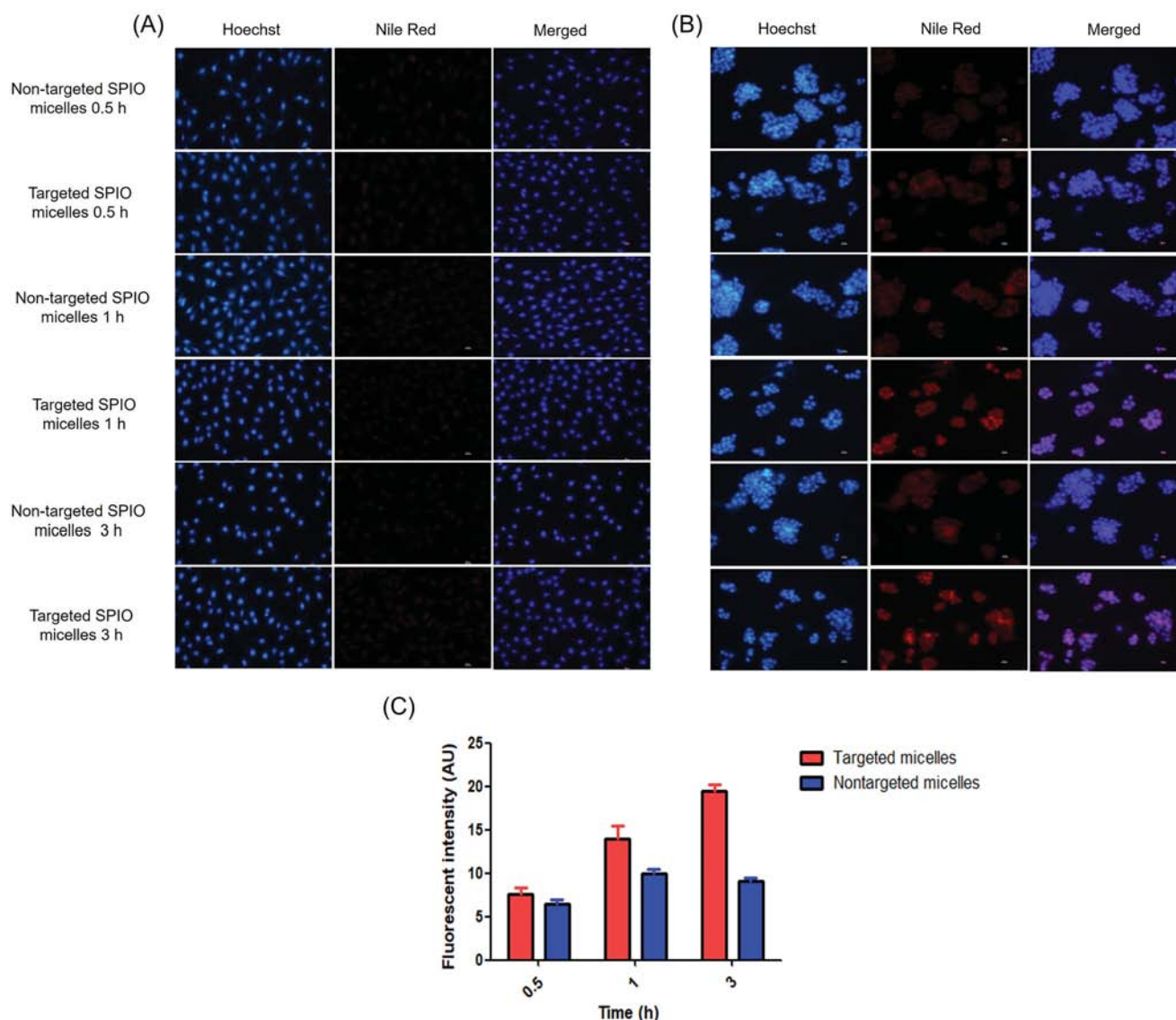


Figure 3. Fluorescence microscopy images of (A) L929 and (B) HepG2 cells incubated 0.5, 1 and 3 h with Nile red SPIO micelles at a Nile red concentration of 0.02 μg . Images show hoechst staining, Nile red staining and merge. (C) Graph illustrates fluorescent intensity (AU) of HepG2 cells incubated at various time points by using Image J. Data represent the mean \pm standard deviation ($n = 3$).

incubation time periods (8, 6, and 4 h). The results demonstrated (Figure 2(B)) that from 8 h, galactose targeted SPIO micelles exerted significant difference ($p < 0.05$) in their activity compared to non-targeted SPIO micelles.

The MTT assay for L929 cells (Figure 2(C)) suggested that blank SPIO micelles and DMSO did not exert any toxic effects at any concentration against normal cells. Figure 2(C) demonstrates that at higher concentration (5, 10.5, and 21 $\mu\text{g}/\text{ml}$), both targeted and non-targeted SPIO micelles showed cytotoxicity effect much higher than that of concentration at 0.5, 1, 1.5, and 2.5 $\mu\text{g}/\text{ml}$. Free drug was toxic to the cells at all concentrations except at the concentration of 0.5 and 1 $\mu\text{g}/\text{ml}$.

3.4. In vitro cellular uptake of Nile red/SPIO micelles

The micelle uptake was observed and evaluated on HepG2 and L929 cells. These cells were incubated with Nile red at the concentration of 0.02 $\mu\text{g}/\text{ml}$ at different incubation time points (0.5, 1, and 3 h). The red colour is from Nile red, whilst the blue image denotes the cells nuclei which were stained by Hoechst dye

(Figure 3(A,B)). As shown in Figure 3(B), as the incubation time elevated from 0.5 to 3 h, images indicated that Nile red-loaded micelles were uptaken by cancer cells. It was observed that the intensity of internalisation of the galactose conjugated micelles augments significantly as time of incubation escalated from 0.5 to 3 h than non-targeted micelles. At 3 h of incubation, a substantial concentration of micelles within cells was noticed; however, very little Nile red was present in the HepG2 cells during 0.5 h of incubation time in both targeted and non-targeted micelles. The cellular uptake data also revealed that there was homogenous spreading of Nile red into the cytoplasm of cells and nuclei at 3 h. During this time period, fluorescence intensity was observed to be more than 0.5 and 1 h. The images demonstrated that galactose targeted micelles are incorporated extensively in the cytoplasmic region and for the non-targeted micelles, the extent of internalisation was markedly less than that of the targeted micelles, whose uptake process can be ascribed through ASPG receptor-mediated endocytic pathway. It was noteworthy that L929 cells displayed little to no red colour from Nile red cellular uptake, suggesting Nile red SPIO micelles were not taken up by

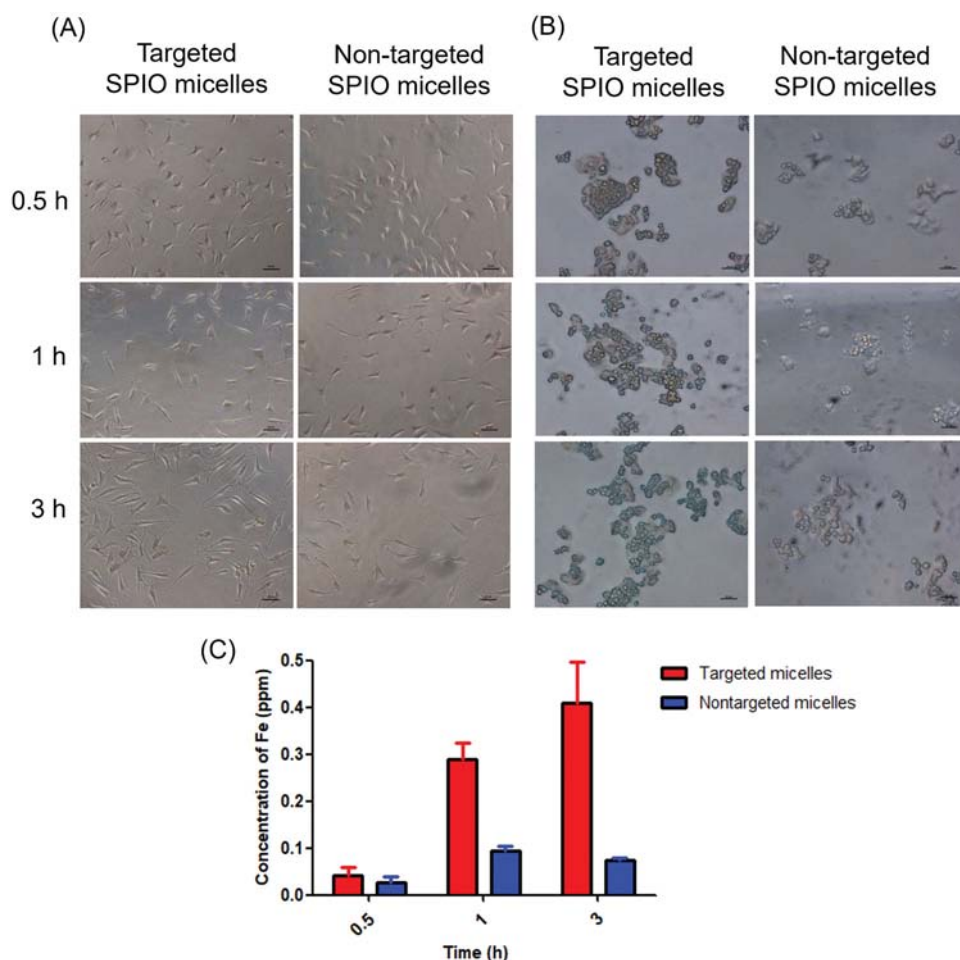


Figure 4. Prussian blue staining of (A) L929 and (B) HepG2 cells that were incubated with targeted and non-targeted SPIO micelles with iron concentration 61 ppm for 0.5, 1, and 3 h and (C) intracellular uptake of Fe at various time periods by FAAS. Data represent the mean \pm standard deviation ($n = 3$).

the normal cells at this time period (Figure 3(A)). This can be attributed to the lack of ASGP receptor expression in the L929 cells. Thus, indicating that Nile red was only taken up by the HepG2 cells. The cellular uptake data substantiate strong and specific binding of the galactose SPIO micelles to HepG2 cells, due to the existence of an abundant ASGPR on the HepG2 cell surface. Nile red dye (hydrophobic dye) has been utilised as tracker and has been prominently enveloped into the hydrophobic core of the micelles for imaging the cellular uptake studies. Nile red exhibits strong fluorescence in hydrophobic milieu, i.e. the core of polymeric micelle. In the aqueous solution, the fluorescence emission intensity was reduced, thus only the fluorescence of Nile red incorporated in the micelles was spotted in the intracellular environment (Majdanski et al. 2018). Cajot et al. (2013) deployed Nile red as a fluorescent probe and encapsulated into the block copolymers for micelle internalisation. SPIO and Nile red were loaded into the polymeric micelles and cellular uptake study demonstrated that the Nile red/SPIO co-loaded micelles were taken up by the cells and steadily increased when the incubation time was extended (Lu et al. 2017; Li W-J et al. 2018).

To further elucidate, ImageJ analysis (Figure 3(C)) was deployed to quantify the cellular uptake study. ImageJ results corroborated the results from fluorescence microscope. At 0.5 h of incubation, no significant uptake of micelles was observed in both targeted and non-targeted micelles, whereas at 3 h, galactose conjugated micelles were significantly internalised to the HepG2 cells than the non-targeted SPIO micelles. Results of

ImageJ confirmed that the cellular uptake of galactose micelles was faster and expeditious than non-targeted micelles at 3 h time period. At 3 h, targeted SPIO micelles demonstrated significantly higher uptake of Nile red in comparison to non-targeted micelles.

3.5. In vitro Prussian blue staining and determination of iron content

Prussian blue staining was carried out to investigate the iron uptake ability of targeted and non-targeted SPIO micelles in HepG2 and L929 cells. These cells were qualitatively visualised by Prussian blue staining and the latter produces characteristics blue colour in the presence of ferric ions. Figure 4(B) unveils that HepG2 cells had higher uptake, shown as more blue deposition, than L929 after incubation at various time periods (Figure 4(A)). It was noteworthy that L929 cells showed little to no blue colour staining at all time period (Figure 4(A)). It also revealed the intense blue colour of SPIO entrapped into the HepG2 cells. At 3 h, results (Figure 4(B)) suggested the uptake of these SPIO in HepG2 cells appeared to be higher. Data also denoted that the micelles were efficaciously taken up into the cells and gradually absorbed when incubation time was prolonged from 0.5 to 3 h. HepG2 cells treated by galactose SPIO micelles exhibited much stronger blue colour than non-targeted SPIO micelles, as ASGPR are over-expressed on HepG2 cells and can mediate galactose micelles effectively, internalising into cells by means of recognition between galactose and ASGPR.

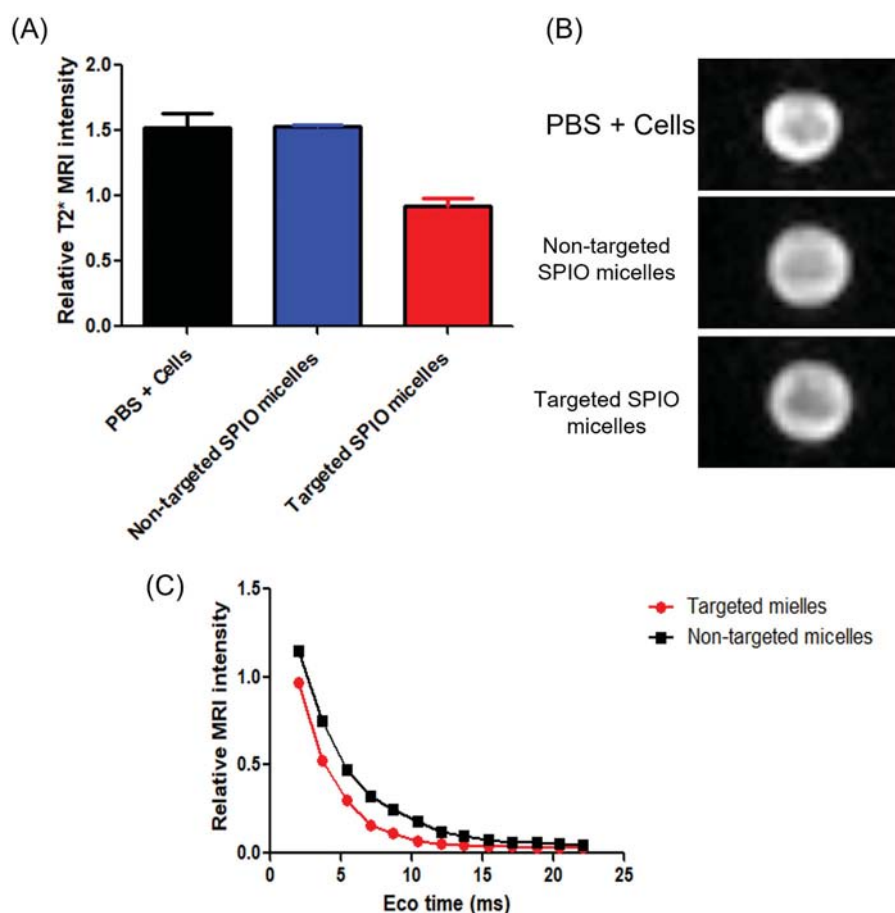


Figure 5. (A) Relative MRI signal intensity of HepG2 treated with PBS + cells, non-targeted SPIO and targeted SPIO micelles for 3 h. (B) T2*-weighted images of PBS with HepG2 cells, non-targeted and targeted SPIO micelles for 3 h of incubation. (C) Curve fitting of signal intensity as function of echo time. Data represent the mean \pm standard deviation ($n = 3$).

Lee et al. (2009) demonstrated SPIO nanoparticles carrying terminal galactose groups exerted more affinity towards ASGPR on the hepatocyte surface and the result showed significantly high SPIO uptake possessing galactose ligand. *In vitro* Prussian blue staining was performed by Li W-J et al. (2018) and it was found that SPIO nanoparticles were effectively taken up by the cells and the amount was escalated as the incubation time was prolonged. Liu et al. (2016) research also focussed on targeting lactobionic acid (galactose moiety) into HepG2 cells and it showed that galactose micelles exhibited much stronger blue colour stain. Our results are congruous with the above researcher's Prussian blue staining data and our findings also substantiate the targeting efficiency of the galactose ligand in HepG2 cells (Figure 3(B)).

Furthermore, for explicating of intracellular iron content of these targeted and non-targeted micelles, FAAS was deployed to study the amount of SPIO taken up by cancer cells. It was noteworthy that the cellular uptake was raised when galactose was conjugated on the surface of SPIO micelles. The data obtained are in consistent to the Prussian blue staining results (Figure 4(B)), suggesting that at 3 h, iron content in the galactose SPIO micelles were significantly higher than non-targeted SPIO micelles.

3.6. *In vitro* MRI

From our Nile red cellular uptake and Prussian blue staining results (Figures 3(B) and 4(B)), it was perceived that the targeting efficacy of galactose targeted SPIO micelles was evident at 3 h and significant in respect to non-targeted SPIO micelles. Hence, it

was decided to investigate the feasibility for tumour targeting by *in vitro* MRI. SPIO has the ability to shorten the hydrogen longitudinal relaxation time (T1) and lower the signal intensity by shortening the hydrogen transverse relaxation time (T2) (Li W-J et al. 2018). These processes enhance the MRI intensity and also expedite the darkening effect of the interfered areas. MRI sensitivity was detected by assessing the transversal relaxation time (T2*) of water proton in tissue-mocking phantom (agarose gel).

At Fe concentration of 61 ppm, HepG2 cells (5×10^5) were treated with galactose targeted and non-targeted SPIO micelles for 3 h. After that HepG2 cells were combined and mixed well with 20 μ l of agarose solution and quickly transferred into 96-well plate for phantom preparation. T2*-weighted MR images of galactose targeted and non-targeted SPIO micelles incubated with HepG2 cells and control (PBS + HepG2 cells) for 3 h and their relative intensity are presented in Figure 5(A,B). The results from the current study indicated that incubation of the HepG2 cells with the galactose targeted SPIO micelles decreased the signal intensity. The enhancement of HepG2 cell uptake by galactose SPIO micelles caused in the darkening effect of MRI images compared to non-targeted micelles and PBS + cells. T2*-weighted image intensity of HepG2 incubated with galactose SPIO micelles after 3 h significantly (one-way ANOVA, $p < 0.05$) declined in respect to non-targeted SPIO micelles and PBS + cells. Figure 5(C) shows the signal intensity as a function of echo time of targeted and non-targeted SPIO micelles. Theerasilp et al. (2017) conducted similar *in vitro* MRI, in which they found when sugar targeted ligand was attached to the SPIO micelles they significantly and

prominently decreased the relative T2* MRI intensity and increased darkening effect of MRI images after 2 h of incubation. When Zhu et al. (2018) conjugated galactose with SPIO loaded nanostructured lipid carrier, they found that these galactose targeted lipid nanocarriers can be employed as a contrast medium and aided in the diagnosis of hepatic diseases. The results from the current study explicit the targeting efficiency of galactose conjugated RSPP050/SPIO micelles.

4. Conclusions

The current study was focused on fabrication of galactose PEG-b-PLA targeted and allyl PEG-b-PLA non-targeted micelles to target HepG2 cells. SPIO contrast agent and hydrophobic drug RSPP050 was concurrently encapsulated into the hydrophobic part of the micelles. RSPP050 loaded micelles exerted inhibitory effect on HepG2 cells. Fluorescence images and Prussian blue staining study revealed that RSPP050 and SPIO could be competently carried into the HepG2 cells by galactose SPIO micelles. Galactose targeted micelles exhibited significant cellular and iron uptake at 3 h in comparison to non-targeted micelles. MRI data also indicated that T2*-weighted image intensity of galactose SPIO micelles after 3 h was less with respect to non-targeted SPIO micelles. Results from the experiments confirmed the efficiency of the theranostic function of galactose RSPP050/SPIO micelles that were the groundwork for *in vivo* study in the future.

Acknowledgements

This research project was supported by Mahidol University. The first author would like to thank Mahidol University, Thailand for supporting via postdoctoral fellowship.

Disclosure statement

The authors declare no conflict of interest.

Funding

This research project is supported by Mahidol University under the New Discovery and Frontier Research Grant.

ORCID

Witaya Sungkarat  <http://orcid.org/0000-0002-2230-1782>
Norased Nasongkla  <http://orcid.org/0000-0001-8739-6260>

References

- Ai H, Flask C, Weinberg B, Shuai X-T, Pagel MD, Farrell D, Duerk J, Gao J. 2005. Magnetite-loaded polymeric micelles as ultrasensitive magnetic-resonance probes. *Adv Mater.* 17(16):1949–1952.
- Bhummaphan N, Nateewattana J, Suksen K, Saeeng R, Chairoungdua A. 2013. Induction of cholangiocarcinoma cells apoptosis by an andrographolide analog. *Sci Res Essays.* 8: 26–31.
- Brigger I, Dubernet C, Couvreur P. 2002. Nanoparticles in cancer therapy and diagnosis. *Adv Drug Deliv Rev.* 54(5):631–651.
- Cajot S, Schol D, Danhier F, Pr  at V, Gillet De Pauw MC, J  r  me C. 2013. *In vitro* investigations of smart drug delivery systems based on redox-sensitive cross-linked micelles. *Macromol Biosci.* 13(12):1661–1670.
- Cheng D, Hong G, Wang W, Yuan R, Ai H, Shen J, Liang B, Gao J, Shuai X. 2011. Nonclustered magnetite nanoparticle encapsulated biodegradable polymeric micelles with enhanced properties for *in vivo* tumor imaging. *J Mater Chem.* 21(13): 4796–4804.
- Ciechanover A, Schwartz AL, Lodish HF. 1983. Sorting and recycling of cell surface receptors and endocytosed ligands: the asialoglycoprotein and transferrin receptors. *J Cell Biochem.* 23(1–4):107–130.
- Eawsakul K, Chinavinijkul P, Saeeng R, Chairoungdua A, Tuchinda P, Nasongkla N. 2017. Preparation and characterizations of RSPP050-loaded polymeric micelles using poly(ethylene glycol)-b-poly(ϵ -caprolactone) and poly(ethylene glycol)-b-poly(D,L-lactide). *Chem Pharm Bull.* 65(6):530–537.
- Ebrahimi E, Khandaghi AA, Valipour F, Babaie S, Asghari F, Motaali S, Abbasi E, Akbarzadeh A, Davaran S. 2016. *In vitro* study and characterization of doxorubicin-loaded magnetic nanoparticles modified with biodegradable copolymers. *Artif Cells Nanomed Biotechnol.* 44(2):550–558.
- El-Serag HB, Rudolph KL. 2007. Hepatocellular carcinoma: epidemiology and molecular carcinogenesis. *Gastroenterology.* 132(7): 2557–2576.
- Fallon RJ, Schwartz AL. 1988. Asialoglycoprotein receptor phosphorylation and receptor-mediated endocytosis in hepatoma cells. Effect of phorbol esters. *J Biol Chem.* 263(26): 13159–13166.
- Fan C, Gao W, Chen Z, Fan H, Li M, Deng F, Chen Z. 2011. Tumor selectivity of stealth multi-functionalized superparamagnetic iron oxide nanoparticles. *Int J Pharm.* 404(1–2):180–190.
- Feng L, Yu H, Liu Y, Hu X, Li J, Xie A, Zhang J, Dong W. 2014. Construction of efficacious hepatoma-targeted nanomicelles non-covalently functionalized with galactose for drug delivery. *Polym Chem.* 5(24):7121–7130.
- Huang C, Li NM, Gao P, Yang S, Ning Q, Huang W, Li ZP, Ye PJ, Xiang L, He DX, et al. 2017. *In vitro* and *in vivo* evaluation of macromolecular prodrug GC-FUA based nanoparticle for hepatocellular carcinoma chemotherapy. *Drug Deliv.* 24(1):459–466.
- Hyodo I, Mizuno M, Yamada G, Tsuji T. 1993. Distribution of asialoglycoprotein receptor in human hepatocellular carcinoma. *Liver.* 13(2):80–85.
- Iacobazzi RM, Porcelli L, Lopodota AA, Laquintana V, Lopalco A, Cutrignelli A, Altamura E, Di Fonte R, Azzariti A, Franco M, et al. 2017. Targeting human liver cancer cells with lactobionic acid-G(4)-PAMAM-FITC sorafenib loaded dendrimers. *Int J Pharm.* 528(1–2):485–497.
- Jayakumar T, Hsieh CY, Lee JJ, Sheu JR. 2013. Experimental and clinical pharmacology of *Andrographis paniculata* and its major bioactive phytoconstituent andrographolide. *Evid Based Complement Alternat Med.* 2013:846740.
- Kumar RA, Sridevi K, Kumar NV, Nanduri S, Rajagopal S. 2004. Anticancer and immunostimulatory compounds from *Andrographis paniculata*. *J Ethnopharmacol.* 92(2–3):291–295.
- Lam T, Pouliot P, Avti PK, Lesage F, Kakkar AK. 2013. Superparamagnetic iron oxide based nanoprobe for imaging and theranostics. *Adv Colloid Interface Sci.* 199–200:95–113.
- Lee CM, Jeong HJ, Kim EM, Kim DW, Lim ST, Kim HT, Park IK, Jeong YY, Kim JW, Sohn MH. 2009. Superparamagnetic iron oxide nanoparticles as a dual imaging probe for targeting hepatocytes *in vivo*. *Magn Reson Med.* 62(6):1440–1446.
- Li W-J, Wang Y, Liu Y, Wu T, Cai W-L, Shuai X-T, Hong G-B. 2018. Preliminary study of MR and fluorescence dual-mode imaging:

- combined macrophage-targeted and superparamagnetic polymeric micelles. *Int J Med Sci.* 15(2):129–141.
- Li H, Yan K, Shang Y, Shrestha L, Liao R, Liu F, Li P, Xu H, Xu Z, Chu PK. 2015. Folate-bovine serum albumin functionalized polymeric micelles loaded with superparamagnetic iron oxide nanoparticles for tumor targeting and magnetic resonance imaging. *Acta Biomater.* 15:117–126.
- Li M, Zhang W, Wang B, Gao Y, Song Z, Zheng QC. 2016. Ligand-based targeted therapy: a novel strategy for hepatocellular carcinoma. *Int J Nanomedicine.* 11:5645–5669.
- Liu X, Lin X, Wu M, Lin R, Li B, Liu J. 2016. SPION@Cu₂-xS nano-clusters for highly sensitive MRI and targeted photothermal therapy of hepatocellular carcinoma. *J Mater Chem B.* 4(23): 4119–4129.
- Lu L, Wang Y, Cao M, Chen M, Lin B, Duan X, Zhang F, Mao J, Shuai X, Shen J. 2017. A novel polymeric micelle used for in vivo MR imaging tracking of neural stem cells in acute ischemic stroke. *RSC Adv.* 7(25):15041–15052.
- Majdanski TC, Pretzel D, Czaplewska JA, Vitz J, Sungur P, Höppener S, Schubert S, Schacher FH, Schubert US, Gottschaldt M. 2018. Spherical and worm-like micelles from fructose-functionalized polyether block copolymers. *Macromol Biosci.* 18(4): e1700396.
- Mazumder A, Assawapanumat W, Dwivedi A, Reabroi S, Chairoungdua A, Nasongkla N. 2019. Glucose targeted therapy against liver hepatocellular carcinoma: in vivo study. *J Drug Deliv Sci Technol.* 49:502–512.
- Nasongkla N, Bey E, Ren J, Ai H, Khemtong C, Guthi JS, Chin S-F, Sherry AD, Boothman DA, Gao J. 2006. Multifunctional polymeric micelles as cancer-targeted, MRI-ultrasensitive drug delivery systems. *Nano Lett.* 6(11):2427–2430.
- Nasongkla N, Shuai X, Ai H, Weinberg BD, Pink J, Boothman DA, Gao J. 2004. cRGD-functionalized polymer micelles for targeted doxorubicin delivery. *Angew Chem Int Ed Engl.* 43(46): 6323–6327.
- Poelstra K, Prakash J, Beljaars L. 2012. Drug targeting to the diseased liver. *J Control Release.* 161(2):188–197.
- Pranatharthihran S, Patel MD, Malshe VC, Pujari V, Gorakshakar A, Madkaikar M, Ghosh K, Devarajan PV. 2017. Asialoglycoprotein receptor targeted delivery of doxorubicin nanoparticles for hepatocellular carcinoma. *Drug Deliv.* 24(1):20–29.
- Puntawee S, Theerasilp M, Reabroi S, Saeeng R, Piyachaturawat P, Chairoungdua A, Nasongkla N. 2016. Solubility enhancement and in vitro evaluation of PEG-b-PLA micelles as nanocarrier of semi-synthetic andrographolide analogue for cholangiocarcinoma chemotherapy. *Pharm Dev Technol.* 21(4):437–444.
- Schleich N, Sibret P, Danhier P, Ucakar B, Laurent S, Muller RN, Jérôme C, Gallez B, Préat V, Danhier F. 2013. Dual anticancer drug/superparamagnetic iron oxide-loaded PLGA-based nanoparticles for cancer therapy and magnetic resonance imaging. *Int J Pharm.* 447(1–2):94–101.
- Sirion U, Kasemsook S, Suksen K, Piyachaturawat P, Suksamrarn A, Saeeng R. 2012. New substituted C-19-andrographolide analogues with potent cytotoxic activities. *Bioorg Med Chem Lett.* 22(1):49–52.
- Situ J-Q, Wang X-J, Zhu X-L, Xu X-L, Kang X-Q, Hu J-B, Lu C-Y, Ying X-Y, Yu R-S, You J, et al. 2016. Multifunctional SPIO/DOX-loaded A54 homing peptide functionalized dextran-g-PLGA micelles for tumor therapy and MR imaging. *Sci Rep.* 6(1): 35910.
- Theerasilp M, Nasongkla N. 2013. Comparative studies of poly(ϵ -caprolactone) and poly(D,L-lactide) as core materials of polymeric micelles. *J Microencapsul.* 30(4):390–397.
- Theerasilp M, Sungkarat W, Nasongkla N. 2018. Synthesis and characterization of SPIO-loaded PEG-b-PS micelles as contrast agent for long-term nanoparticle-based MRI phantom. *Bull Mater Sci.* 41(2):42.
- Theerasilp M, Sunintaboon P, Sungkarat W, Nasongkla N. 2017. Glucose-installed, SPIO-loaded PEG-b-PCL micelles as MR contrast agents to target prostate cancer cells. *Appl Nanosci.* 7(8): 711–721.
- Thitichai N, Thanapongpibul C, Theerasilp M, Sungkarat W, Nasongkla N. 2019. Study of biodistribution and systemic toxicity of glucose functionalized SPIO/DOX micelles. *Pharm Dev Technol.* 24(8):935–946.
- Voon SH, Kue CS, Imae T, Saw WS, Lee HB, Kiew LV, Chung LY, Yusa SI. 2017. Doxorubicin-loaded micelles of amphiphilic diblock copolymer with pendant dendron improve antitumor efficacy: in vitro and in vivo studies. *Int J Pharm.* 534(1–2): 136–143.
- Xiao RZ, Zeng ZW, Zhou GL, Wang JJ, Li FZ, Wang AM. 2010. Recent advances in PEG-PLA block copolymer nanoparticles. *Int J Nanomedicine.* 5:1057–1065.
- Yang H-K, Bao J-F, Mo L, Yang R-M, Xu X-D, Tang W-J, Lin J-T, Wang G-H, Zhang L-M, Jiang X-Q. 2017. Bioreducible amphiphilic block copolymers based on PCL and glycopolypeptide as multifunctional theranostic nanocarriers for drug delivery and MR imaging. *RSC Adv.* 7(34):21093–21106.
- Yoo HS, Lee EA, Park TG. 2002. Doxorubicin-conjugated biodegradable polymeric micelles having acid-cleavable linkages. *J Control Release.* 82(1):17–27.
- Zhu X, Deng X, Lu C, Chen Y, Jie L, Zhang Q, Li W, Wang Z, Du Y, Yu R. 2018. SPIO-loaded nanostructured lipid carriers as liver-targeted molecular T2-weighted MRI contrast agent. *Quant Imaging Med Surg.* 8(8):770–780.